Novel mechanism for vorticity generation in black-hole accretion disks

Chinmoy Bhattacharjee,[1,2] Rupam Das,[3] and S. M. Mahajan[4,2,5]

[1]*Institute for Fusion Studies, The University of Texas at Austin, Austin, Texas 78712, USA*
[2]*Department of Physics, The University of Texas at Austin, Austin, Texas 78712, USA*
[3]*Department of Physical and Applied Sciences, Madonna University, Livonia, Michigan 48150, USA*
[4]*Institute for Fusion Studies, The University of Texas at Austin, Austin, Texas 78712, USA*
[5]*Shiv Nadar University, NH91, Tehsil Dadri, Gautam Buddha Nagar, Uttar Pradesh, 201 314, India*
(Received 2 April 2015; published 4 June 2015)

Vorticity generation in accretion disks around Schwarzschild and Kerr black holes is investigated in the context of magnetofluid dynamics derived for both General Relativity (GR) and modified gravity formulations. In both cases, the Kerr geometry leads to a "stronger" generation of vorticity than its Schwarzschild counterpart. Of the two principal sources, the relativistic drive peaks near the innermost stable circular orbit (isco), whereas the baroclinic drive dominates at larger distances. Consequences of this new relativistic vorticity source are discussed in several astrophysical settings.

DOI: 10.1103/PhysRevD.91.123005 PACS numbers: 97.60.Lf, 04.20.-q, 04.50.Kd

I. INTRODUCTION

An exploration of the dynamics of accretion disks near compact astrophysical objects can advance our understanding of phenomena as diverse as angular momentum transport, jet production, and gamma ray bursts [1–6]. Baroclinic instability arising from misalignment between temperature and entropy gradients in a hot charged fluid rotating in an accretion disk is considered to be one of the most probable pathways for vorticity generation in astrophysics [7–10]. Such vortices (electromagnetic and hydrodynamic) can be amplified through several mechanisms such as dynamos and magnetorotational instability (MRI) leading to a large scale vortical field [11–13]. The resulting vortical field geometry can be responsible for angular momentum transport and production, acceleration and collimation of jets in black holes, protostars, microquasars, etc. [5,7].

In this paper, we will explore additional sources of vorticity generation that can contribute to angular momentum transport, jet production, and collimation as well as broaden our understanding of black hole accretion, in general. Unlike the traditional "baroclinic" mechanism, these additional drives depend on the relativistic effects—both special and general. Vorticity generation (via the relativistic drives) in the accretion disk near the Schwarzschild black hole was, previously, studied for a generalized "magnetofluid" in curved space-time [14]. The relativistic drive for a pure barotropic system naturally emerges in the dynamics of a magnetofluid, combining kinematic and thermodynamical attributes of a hot fluid.

Let us begin by recapturing the salient features of the magnetofluid formalism and of earlier work on relativistic drives:

1) The essence of the magnetofluid formalism (for a perfect fluid) lies in the construction of an antisymmetric, hybrid tensor [15]

$$M^{\mu\nu} = F^{\mu\nu} + (m/q)S^{\mu\nu}, \tag{1}$$

that is a weighted sum of the electromagnetic field tensor $F^{\mu\nu}$ (weight = charge q), and the composite (kinematic-statistical) fluid tensor $S^{\mu\nu} = \nabla^\mu(\mathcal{G}U^\nu) - \nabla^\nu(\mathcal{G}U^\mu)$ (weight = mass m) [15,16]. The statistical factor $\mathcal{G}$ is the thermodynamic enthalpy. In terms of $M^{\mu\nu}$, the entire dynamics of the relativistic hot fluid is expressible in the succinct equation (T is the temperature of the fluid)

$$qU_\nu M^{\mu\nu} = \frac{\nabla^\mu p - mn\nabla^\mu \mathcal{G}}{n} = T\nabla^\mu \sigma, \tag{2}$$

where the right-hand side is the thermodynamic force expressed in terms of the fluid entropy σ using the standard thermodynamic relation between entropy with enthalpy. Here, U^μ and n represent, respectively, the plasma 4-velocity and the number density.

2) The 3-vector part of (2) reduces to the more familiar form of 3D vortex dynamics except that the standard fluid vorticity is replaced by the hybrid magnetofluid vorticity. The addition of relativity, however, introduces a fundamental change; the topological helicity invariant $\mathcal{H} = \langle \vec{\Omega} \cdot \nabla \times^{-1} \vec{\Omega} \rangle$ (with $\vec{\nabla} \times^{-1} \vec{\Omega}$ being the inverse curl of vorticity) of an ideal nonrelativistic fluid no longer pertains.

Through the "distortion" of space-time, relativistic dynamics breaks the helicity invariant even in ideal dynamics ($\sigma = \sigma(T)$); new sources and sinks appear, and the creation and destruction of the generalized vorticity become possible in ideal dynamics [14,15,17,18]. Such sources can, therefore, be available to create vorticity in the accretion disk.

3) Recently, this formalism was generalized to incorporate nonminimal coupling of the magnetofluid to a curved background space-time [19]. It is quite remarkable that the nonminimal coupling [introduced through $f_m(R)$, a

 © 2015 American Physical Society

function of the Ricci scalar R] changes the equation of motion (2) only minimally

$$qU_\nu \mathcal{M}^{\mu\nu} = QT\nabla^\mu \sigma; \tag{3}$$

it multiplies the right-hand side with a curvature dependent factor $Q = (1 + \lambda f_m(R))$ that reduces to unity as the nonminimal part goes to zero, as expected. This has also resulted in the introduction of additional gravity-coupled flow field tensor which, after appropriate $3+1$ decomposition, yields new expressions for generalized electric and magnetic field. The formalism, epitomized in Eqs. (2) and (3), will be, henceforth, called magnetofluid formalism.

In this paper, then, we will investigate vorticity generation in accretion disk for minimally as well as nonminimally coupled magnetofluid in Schwarzschild and Kerr space-time. The magnitude of induced vorticity will be estimated in the special case when matter and space-time are coupled with constant Ricci scalar R_0, the simplest functional form of nonminimal coupling.

We first give a summary of the derivation of generalized equation of motion of a new hybrid magnetofluid in curved background space-time. Next, the Arnowitt–Deser–Misner (ADM) formalism of electrodynamics [20–23] presented in Appendix is applied to this new formulation of magnetofluid, and the equations obtained are cast into the vorticity evolution equation. These equations are analyzed for accretion disks to calculate and estimate generalized vorticity. Finally we compare the relativistic drives with the more conventional baroclinic drive.

II. MAGNETOFLUID FORMALISM

The modified theory of gravity offers an alternative approach to explain the inferred accelerated expansion of the Universe and other cosmological data by introducing deviations from Einstein's GR. The so-called $f(R)$ gravity modifies GR in the low energy (curvature) regime, but its behavior in the high energy regime has also been the topic of current research [24–26]. To expand the scope of our earlier calculations, we incorporate the $f(R)$ gravity [through the term $\lambda f(R)$] in the magnetofluid formalism. Referring the reader to Ref. [19] for a detailed derivation, we simply write down, here, the two main equations: the modified Einstein equation ($G = c = 1$)

$$(1 + F_g(R))R^{\mu\nu} - \frac{1}{2}(R + f_g(R))g^{\mu\nu} - (\nabla^\mu\nabla^\nu - g^{\mu\nu})F_g(R) = 8\pi T^{\mu\nu}_{\text{total}} \tag{4}$$

and the magnetofluid equation of motion

$$(1 + \lambda f_m(R))\nabla_\mu T^{\mu\nu}_{pf} = [qnF^\nu{}_\beta U^\beta - \lambda F_m(R)(T^{\mu\nu}_{pf} + g^{\mu\nu}\rho)\nabla_\mu R], \tag{5}$$

where $F_g = f_g{}'(R)$, R is the Ricci scalar and $T^{\mu\nu}_{\text{total}}$ is the total stress-energy tensor for both the perfect fluid and Maxwell's field in curved space-time. In the preceding equations, q is the charge of the particle, and $T^{\mu\nu}_{pf} = (p+\rho)U^\mu U^\nu + pg^{\mu\nu}$ (with $U^\mu = dx^\mu/d\tau$) is the energy-momentum tensor for a perfect isotropic fluid; τ is the proper time. The phenomenological parameter λ represents the coupling strength of the plasma to its background geometry, now modified through $f_m(R)$ and $F_m(R) = f'_m(R)$. The quantity $p + \rho = h$ is the enthalpy of the fluid plasma and often appears in the formalism as the combination $\mathcal{G} = h/mn$ with m, n, ρ, and p being the mass, number density, energy density, and pressure, respectively.

Notice that the equation of motion (5) is not yet in the promised "canonical" form (3). To make progress, following Refs. [15,19], we will construct the new grand unified vorticity tensor $\mathcal{M}^{\mu\nu}$ that reflects nonminimal coupling. After some patient algebra, we find that $\mathcal{M}^{\mu\nu}$ is again the weighted sum [as (2)],

$$\mathcal{M}^{\mu\nu} = F^{\mu\nu} + \frac{m}{q}D^{\mu\nu}, \tag{6}$$

but with a considerably more complicated

$$D^{\mu\nu} = (1 + \lambda f_m(R) - \lambda R F_m)S^{\mu\nu} + \frac{m}{q}\lambda F_m K^{\mu\nu} \tag{7}$$

replacing $S^{\mu\nu} = \nabla^\mu(\mathcal{G}U^\nu) - \nabla^\nu(\mathcal{G}U^\mu)$. We needed to "find" a new curvature-weighted antisymmetric flow field tensor

$$K^{\mu\nu} = \nabla^\mu(R\mathcal{G}U^\nu) - \nabla^\nu(R\mathcal{G}U^\mu), \tag{8}$$

to derive the sought-after form. The new fluid tensor $D^{\mu\nu}$ contains, explicitly, the coupling of flow field to gravity. Thus, the dynamics of a hot fluid system in curved background space-time can be written into the canonical four-dimensional (4D) vortex form

$$qU_\nu \mathcal{M}^{\mu\nu} = (1 + \lambda f_m(R))T\nabla^\mu \sigma, \tag{9}$$

the form advertised in (3). We have "assumed" that the standard thermodynamic relations continue to hold; it is, of course, contingent upon an appropriately well-defined local concept of temperature in curved space-time.

Notice that, when $\lambda = 0$, $\mathcal{M}^{\mu\nu}$ reduces to its minimally coupled counterpart tensor $M^{\mu\nu}$ defined in Refs. [14,15].

Equation (9) is the main result that describes the magnetofluid dynamics in curved space-time. It reveals that a charged relativistic fluid, coupled nonminimally to gravity, obeys a 4D vortex dynamics like its gravity free and minimally coupled (to gravity) counterparts. The new grand vorticity tensor subsumes earlier limiting cases in a transparent manner.

We would now apply the above formulation to investigate the vorticity generation in accretion disks around

black holes. To do calculations in terms of familiar quantities, an appropriate $3+1$ decomposition of the space-time is necessary; it is presented in Appendix. Next, we present the 3D vortical dynamics in order to facilitate computation of vorticity generation.

A. Vortical dynamics

With the $3+1$ decomposition presented in Appendix, the spacelike projection, i.e., $\gamma^{\beta}{}_{\mu}$ projection of the unified field equation of motion (9), gives us the momentum evolution equation

$$\alpha q\Gamma\vec{\xi} + q\Gamma(\vec{v}\times\vec{\Omega}) = -(1+\lambda f_m(R))T\vec{\nabla}\sigma, \tag{10}$$

whereas the timelike (n_μ) projection gives the equation of energy conservation

$$\alpha q\Gamma\vec{v}\cdot\vec{\xi} = T(1+\lambda f_m(R))(\mathcal{L}_t\sigma - \vec{\beta}\cdot\vec{\nabla}\sigma), \tag{11}$$

where $\vec{\xi}$ and $\vec{\Omega}$ are, respectively, the generalized electric and magnetic fields given by Eqs. (A6) and (A7) in Appendix. Also, α, Γ, and $\vec{v}$ are defined in Eqs. (A1), (A2), and (A3). Sources responsible for magnetic field generation, in particular, the sources that are gravity driven, can be derived from the generalized vorticity evolution equation (which is really the generalized Faraday's law) by manipulating Eq. (10).

Since $\mathcal{M}^{\mu\nu}$ is an antisymmetric tensor, the divergence of its dual is zero, i.e., $\nabla_\mu\mathcal{M}^{*\mu\nu} = 0$. Taking the $\gamma^{\beta}{}_{\mu}$ projection of the preceding identity, we derive

$$\mathcal{L}_t\vec{\Omega} = \mathcal{L}_{\vec{\beta}}\vec{\Omega} - \vec{\nabla}\times(\alpha\vec{\xi}) - \alpha\Theta\vec{\Omega}, \tag{12}$$

where $\mathcal{L}$ denotes Lie derivatives with $\mathcal{L}_t = \partial_t$ along t^μ, $\mathcal{L}_{\vec{\beta}}\vec{\Omega} = [\vec{\beta},\vec{\Omega}]$, and the expansion factor Θ is defined in Appendix.

It should be noted that, even in the absence of nonminimal coupling to gravity ($\lambda = 0$), (minimal) coupling to gravity still manifests in the formalism. Equation (12), in conjunction with Eq. (10), gives us the vorticity evolution equation

$$\begin{aligned}\mathcal{L}_t\vec{\Omega} - \vec{\nabla}\times(\vec{v}\times\vec{\Omega}) - \mathcal{L}_{\vec{\beta}}\vec{\Omega} + \alpha\Theta\vec{\Omega}\\ = \vec{\nabla}\times\left(\frac{T}{q\Gamma}(1+\lambda f_m(R))\vec{\nabla}\sigma\right).\end{aligned} \tag{13}$$

All terms on the left-hand side operate on the vorticity 3-vector $\vec{\Omega}$ while the right-hand side provides, just as in the conventional picture, possible sources for vorticity generation. The left-hand side, however, has lot more structure than the conventional 3D vortex dynamics; the first two terms reflect the standard Helmholtz vortical dynamics, while $\alpha\Theta\vec{\Omega}$ and $\mathcal{L}_{\vec{\beta}}\vec{\Omega}$, are nontrivial gravity modifications. Thus, the gravity coupling does, fundamentally, modify the projected 3D vortex dynamics, in spite of the fact that the 4D vortex equations have exactly the same form.

III. VORTICITY GENERATION

To apply the formalism to vorticity generation in astrophysics, specifically in accretion disks around compact objects like Schwarzschild and Kerr black holes, we have to specify the space-time geometry, the space-time metric that controls the motion of plasma particles. The standard metric describing the stationary and axially symmetric (or spherically symmetric) space-time for Kerr (or Schwarzschild) black holes can be written as [27]

$$ds^2 = g_{tt}dt^2 + 2g_{t\phi}dtd\phi + g_{rr}dr^2 + g_{\theta\theta}d\theta^2 + g_{\phi\phi}d\phi^2. \tag{14}$$

The exploration of geodesic motions of plasma in accretion disks will allow us to compute various relevant physical quantities. Since we are interested only in the timelike geodesics in thin accretion disks, the Euler–Lagrange equations can be derived from the Lagrangian for the above stationary and axisymmetric space-time, $2L = ds^2/d\tau^2 = -1$, with τ being the proper time along timelike geodesics. Thus, the corresponding Euler–Lagrangian equations describing the timelike geodesics in the equatorial plane take the form ([27])

$$\frac{dt}{d\tau} = \frac{\tilde{E}g_{\phi\phi} + \tilde{L}g_{t\phi}}{g_{t\phi}^2 - g_{tt}g_{\phi\phi}}, \tag{15}$$

$$\frac{d\phi}{d\tau} = -\frac{\tilde{E}g_{t\phi} + \tilde{L}g_{tt}}{g_{t\phi}^2 - g_{tt}g_{\phi\phi}}, \tag{16}$$

$$g_{rr}\left(\frac{dr}{d\tau}\right)^2 = -1 + \frac{\tilde{E}^2 g_{\phi\phi} + 2\tilde{E}\,\tilde{L}\,g_{t\phi} + \tilde{L}^2 g_{tt}}{g_{t\phi}^2 - g_{tt}g_{\phi\phi}} \equiv V_{\rm eff}, \tag{17}$$

where $\tilde{E}$ and $\tilde{L}$ are specific energy and specific angular momentum, respectively. For stable circular orbits in the equatorial plane, using $V_{\rm eff} = 0$ and $dV_{\rm eff}/dr = 0$, the constants of motion including angular velocity ω are found to be

$$\tilde{E} = -\frac{g_{tt} + g_{t\phi}\omega}{\sqrt{-g_{tt} - 2g_{t\phi}\omega - g_{\phi\phi}\omega^2}}, \tag{18}$$

$$\tilde{L} = \frac{g_{t\phi} + g_{\phi\phi}\omega}{\sqrt{-g_{tt} - 2g_{t\phi}\omega - g_{\phi\phi}\omega^2}}, \tag{19}$$

$$\omega = \frac{d\phi}{dt} = \frac{-g_{t\phi,r} + \sqrt{(g_{t\phi,r})^2 - g_{tt,r}g_{\phi\phi,r}}}{g_{\phi\phi,r}}. \quad (20)$$

The Lorentz factor for particles can be derived from

$$\Gamma = \frac{\tilde{E}g_{\phi\phi} + \tilde{L}g_{t\phi}}{g_{t\phi}^2 - g_{tt}g_{\phi\phi}} = \frac{1}{\sqrt{-g_{tt} - 2g_{t\phi}\omega - g_{\phi\phi}\omega^2}}. \quad (21)$$

Moreover, for any given scalar function P, the gradient is defined as

$$\vec{\nabla}P = \frac{1}{\sqrt{g_{rr}}}\partial_r P\hat{e}_r + \frac{1}{\sqrt{g_{\theta\theta}}}\partial_\theta P\hat{e}_\theta + \frac{1}{\sqrt{g_{\phi\phi}}}\partial_\phi P\hat{e}_\phi. \quad (22)$$

Next, we assume a thin accretion disk with zero latitudinal speed $v_\theta = 0$ for the plasma; we will also assume that the radial velocity of the plasma is negligible compared to the orbital velocity $v_\phi \gg v_r$. The orbits of the plasma constituents are also taken to be almost circular ($\dot{r} \approx 0$). Since our formalism is based on perfect fluid, we can also assume the plasma to be barotropic with its pressure depending on density only, i.e., $\sigma = F(T)$. Then, with this assumption, we can write the relation between the temperature and entropy gradient as $T\vec{\nabla}\sigma = \chi k_b \vec{\nabla}T$, which evidently will cause the baroclinic drive N_B to vanish, where χ is a dimensionless quantity of order unity.

To compute the appropriate temperature profile in the region of interest in the accretion disk, we follow the prescription presented by Novikov and Thorne [28]. It turns out that, for $M = 14.3M_\odot$ and $\dot{M} = 0.472 \times 10^{19}\ \mathrm{gs}^{-1}$, the inner- and outermost stable circular orbits (average width of the accretion disk) are located mostly in the optically thick region of the accretion disk; this is true for both geometries. Therefore, for an optically thick region, using the Stefan–Boltzmann law, the temperature profile can be written as [26,27]

$$T(r) = z\left(\frac{\mathfrak{f}(r)}{\sigma_{\mathrm{SB}}}\right)^{\frac{1}{4}}, \quad (23)$$

where σ_{SB} is the Stefan–Boltzmann constant and z is redshift due to gravitational effects. For $\theta = \pi/2$, and for a vanishing disk inclination angle, the redshift can be written as $1 + z = \Gamma$. Here, $\mathfrak{f}(r)$ is the energy flux for a relativistic accretion disk presented in Refs. [26,29] by Page and Thorne as

$$\mathfrak{f}(r) = -\frac{\dot{M}_0}{4\pi\sqrt{-g}}\frac{\omega_{,r}}{(\tilde{E} - \omega\tilde{L})^2}\int_{r_{\mathrm{isco}}}^{r}(\tilde{E} - \omega\tilde{L})\tilde{L}_{,r}dr, \quad (24)$$

where r_{isco} is the radius of the innermost stable circular orbit in the accretion disk and $\dot{M}_0$ is the mass accretion rate.

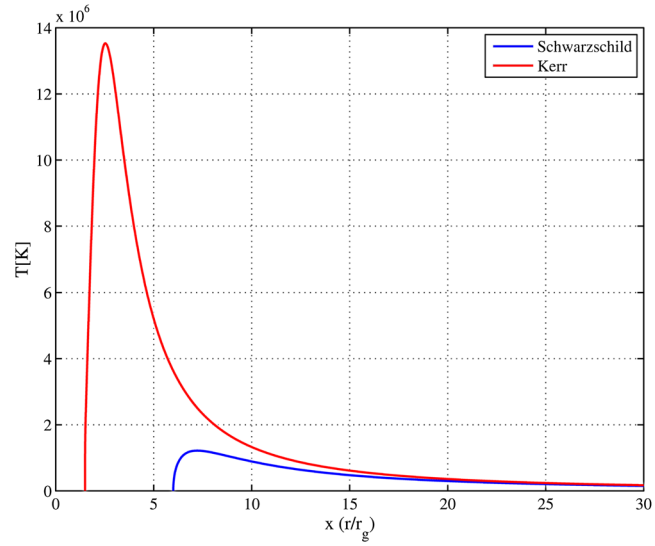

FIG. 1 (color online). Temperature profile for the Schwarzschild (blue) and Kerr black hole (red) from $x = 1.5$ to $x = 30$.

The temperature and the Lorentz factor profiles, displayed, respectively, in Figs. 1 and 2, reveal similar general features for the Kerr space-time: increasing from their corresponding value at r_{isco}, they reach a peak at some radius and then monotonically decrease as we move away from the center of the corresponding black holes [30]. However, only the temperature profile in the Schwarzschild geometry shares the similar feature. These features of the temperature and the gamma (Γ) profiles will manifest in the vorticity generation as well as in the relative strength between the corresponding relativistic and classical drives.

Throughout this paper, we will use parameters obtained from observation on the Galactic black hole Cygnus-XI as

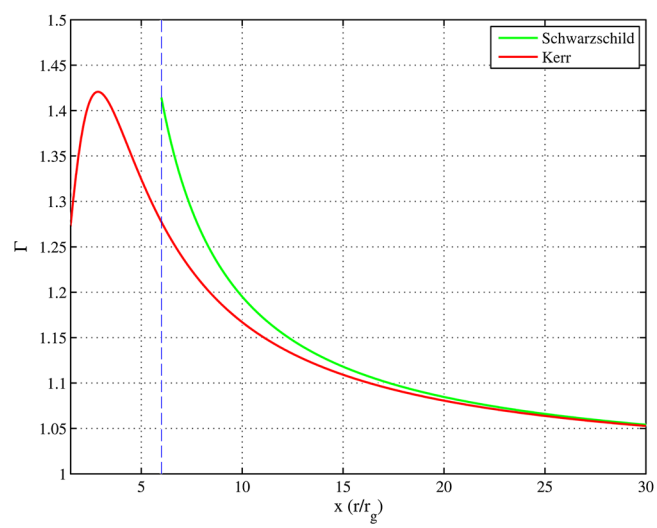

FIG. 2 (color online). Lorentz factor for Schwarzschild (green) and Kerr black hole (red) from $x = 1.5$ to $x = 30$. The dashed line (blue) indicates innermost circular orbit (isco) for the Schwarzschild blackhole.

representative, $M = 14.38 M_\odot$, $\dot{M} = 0.472 \times 10^{19}\ \mathrm{gs}^{-1}$, and $a = 0.99 r_g$, where M and a are, respectively, the mass and angular momentum per unit mass of the black hole [31,32]. Figure 1 shows the temperature profile in Kerr (Schwarzschild) geometry from $r = 1.5 r_g$ ($r = 6 r_g$) to $r = 30 r_g$ with $r_g = GM/c^2$ in the normalized unit of $x = r/r_g$. The profile shows a peak temperature between 10^6–$10^7 K$ which drops as we move from the event horizon radially outward. These profiles are used in this paper to calculate the vorticity generation in the accretion disk.

A. Schwarzschild geometry

For a spherically symmetric and static space-time (Schwarzschild space-time), the above vortical evolution equation (13) reduces to the one presented in Ref. [14], i.e., $\mathcal{L}_t \vec{\Omega} - \vec{\nabla} \times (\vec{v} \times \vec{\Omega}) = \vec{\nabla} \times ((T/q\Gamma)\vec{\nabla}\sigma)$. Since the spherically symmetric and static space-time can be foliated without any shift function $\vec{\beta}$, and the foliation obeys the time translation symmetry leading to a vanishing extrinsic curvature, the new term involving Θ on the left-hand side disappears. Thus, the structure is precisely like the 3D vortex dynamics. The simplified vortical evolution equation can be used to approximately compute the weak field seed generation in the hot fluid system in the accretion disk in Schwarzschild geometry.

The relevant space-time metric elements are

$$g_{tt} = -\alpha^2 = -\left(1 - \frac{2r_g}{r}\right); \qquad g_{rr} = \left(1 - \frac{2r_g}{r}\right)^{-1},$$
$$g_{\theta\theta} = r^2; \qquad g_{\phi\phi} = r^2 \sin^2\theta. \tag{25}$$

Then, using the Eqs. (18)–(21), we can calculate the orbital velocity and gamma factor for the orbital motion of plasma in the accretion disk. Since the radial velocity of the plasma is assumed to be negligible compared to the orbital velocity $v_\phi \gg v_r$, the orbits of the plasma elements are taken to be almost circular ($\dot{r} \approx 0$). Then, inserting the Schwarzschild metric elements, (25), in Eqs. (15)–(17) and imposing $V_{\mathrm{eff}} = 0$ and $dV_{\mathrm{eff}}/dr = 0$ reveals that there exists one stable circular orbit at $x > 6$ and one unstable circular orbit at $6 > x > 3$ [22]. This also dictates the applicability of the temperature profile in accretion disk. The temperature profile used in this paper is valid in the region of stable circular orbits.

B. Kerr geometry

For an axisymmetric (but not spherically symmetric) stationary system, like the Kerr black hole, our previous assumption of the zero shift function, $\vec{\beta} = 0$, is no longer valid. Consequently, the pertinent equation (13), in general, does not show any similarity to standard 3D vortex dynamics. The shift function for rotating black holes can be taken to be $\vec{\beta} = -\omega\, \hat{e}_\phi$ with respect to a zero angular momentum observer. The term involving the shift function, however, will give zero contribution since we assume that both ω and Ω have only radial dependence. In addition, it can be further shown that the term involving the expansion factor Θ vanishes. Thus, the vorticity evolution equation, even for Kerr geometry, will resemble the standard 3D vortex dynamics.

The relevant space-time metric elements in Boyer–Lindquist coordinates are [26]

$$g_{tt} = -\alpha^2 = -\frac{(\Delta_r - a^2)}{r^2}; \qquad g_{rr} = \frac{r^2}{\Delta_r},$$
$$g_{t\phi} = -\frac{2a}{r^2}(r^2 + a^2 - \Delta_r); \qquad g_{\phi\phi} = \frac{(r^2 + a^2)^2 - \Delta_r a^2}{r^2}, \tag{26}$$

where $\Delta_r = (r^2 + a^2) - 2r_g r$. Then, again inserting the Kerr metric elements, (26), in Eqs. (15)–(17) and imposing $V_{\mathrm{eff}} = 0$ and $dV_{\mathrm{eff}}/dr = 0$ reveals that the innermost circular orbit in the Kerr black hole is located at $x = 1.4545$ for $a = 0.99 r_g$, which was taken into account in deriving the temperature profile for the accretion disk in Kerr geometry. Note that we will assume $a = 0.99 r_g$ throughout the rest of the paper.

C. Computing vorticity

For both Schwarzschild and Kerr configurations, computation of vorticity generation requires knowledge of the ϕ dependence of the temperature profile. However, the most commonly used temperature profiles (including the GR corrected ones) for accretion disks show only radial dependence. Previously, an estimate of vorticity generation was computed using an average temperature of the accretion disk [14]. However, as shown in Fig. 1, General Relativity restricts the application of an average disk temperature throughout the disk as it involves regions of unstable orbits leading to nonlinear behavior. Moreover, plasmas orbiting in accretion disks for both black hole configurations undergo gravitational radiation reaction, which for a Kerr black hole can cause a plasma particle to lose as much as 42% of its initial energy as it approaches the event horizon [22].

Toroidal temperature dependence is created due to the gravitational radiation by the orbiting plasma particles; the induced radiation reaction, in turn, makes the stable circular orbits deviate slightly from geodesic motion [22]. A particle, initially in a circular orbit at $x > 6$ ($x > 1.4545$) for the Schwarzschild (Kerr) metric, slowly spirals into smaller nearly circular orbits as it radiates energy until it reaches the orbital radius $x = 3$ ($x = 1.4545$), where the orbit becomes unstable. Therefore, the stable circular orbits do not close in either geometry, and, depending on the magnitude of radiation reaction, the spatial orbital trajectory in the equatorial plane is assumed to be represented by

$r = r(\phi)$, a solution to the geodesic equation relating coordinates r to ϕ.

Next, we assume, without loss of generality, that the orbits of the spiraling plasma elements in the disk can be approximated by $r(\phi) = r_0 e^{-\zeta\phi}$, where r_0 is the initial radial distance of the plasma particles from the center of the black hole and ζ is the parameter that controls how tightly a nearly circular orbit spirals around the black hole. In general, the factor ζ can be a complicated function of black hole mass as well as the energy and the angular momentum of plasma elements. Determined from the geodesic equation relating coordinates r to ϕ with appropriate boundary conditions, ζ can be a function of the radial distance. However, since our focus is on the region of accretion disk over which the timelike geodesic orbits of the plasma elements are closely bound, we can assume the spiraling parameter ζ to be a constant. A rapidly varying spiral with varying ζ will contribute more to the vorticity as can be seen from Eq. (27).

As mentioned earlier, the radiation reaction can be the source for slight deviations from the closed stable circular orbit, thereby imparting temperature variations around a spirally circular orbit. Thus, for the spiral orbit, $r(\phi) = r_0 e^{-\zeta\phi}$, $\partial T/\partial\phi = (\partial T/\partial r)(dr/d\phi) = -\zeta r(\partial T/\partial r)$, and the seed vortical field $|\vec{\Omega}|$ may be estimated as

$$\vec{\Omega}(r) = -\frac{\chi k_b c r \zeta}{q} \frac{1}{\sqrt{g_{rr} g_{\phi\phi}}} \partial_r(\Gamma^{-1})(\partial_r T)\Delta t \hat{\theta}, \tag{27}$$

where Δt is the characteristic time for linear vorticity generation under which the changes in space-time geometry are negligible. Therefore, we choose this time scale to be $\Delta t = 2\pi/\omega$, and, as expected, this coordinate time interval Δt is related to the proper time interval $\Delta\tau$ by $\Delta t = \Gamma\Delta\tau$. For an observer far away from the accretion disk under observation, these two time intervals are practically the same. For the Schwarzschild geometry, Eq. (27) simplifies to

$$\vec{\Omega}(x) = -\frac{3\zeta k_b \pi \Gamma \alpha \chi}{q\sqrt{x} r_g} \partial_x T \hat{\theta}, \tag{28}$$

$x = r/r_g$ is the normalized distance, and $q = -e$ is the electron charge.

Figures 3 and 4 show the radial dependence of the magnitude of the vorticity generated in the accretion disk plasmas embedded in Schwarzschild and Kerr geometries for three different choices of ζ. Both figures show a drastic reduction in $|\Omega|$ as the temperature maxima are approached (temperature gradient going to zero), and then $|\Omega|$ picks up as we go over to the other side of the maximum. In addition, the existence of a second dip in the Kerr vorticity profile can be attributed to the vanishing of the gradient of the corresponding Lorentz factor. Therefore, the effect of the relevant gamma and temperature gradients indicates a distinct vorticity profile in Kerr space-time, where vorticity changes direction twice before it gradually decays radially outward in the disk.

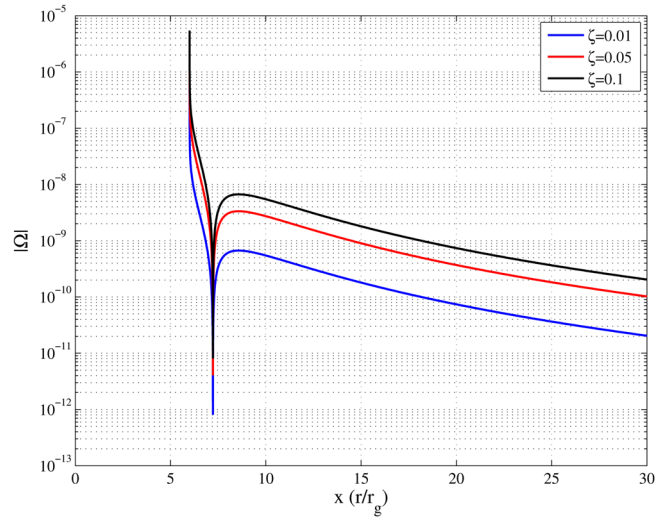

FIG. 3 (color online). Vorticity magnitude (in the units of Gauss) for the Schwarzschild black hole with different ζ values between $6.0r_g$ and $30r_g$ for $M = 14.8M_\odot$.

However, as we move radially outward in the disk, both induced vorticities decrease almost at the same rate, maintaining their difference.

D. Black hole accretion disk in modified gravity

The results of last section were derived for the accretion disk fluid minimally coupled to standard GR. We will now explore the changes in vorticity generation brought about by modified gravity, more precisely, by the simplest functional form of $f(R) = R_0 =$ constant. Following the

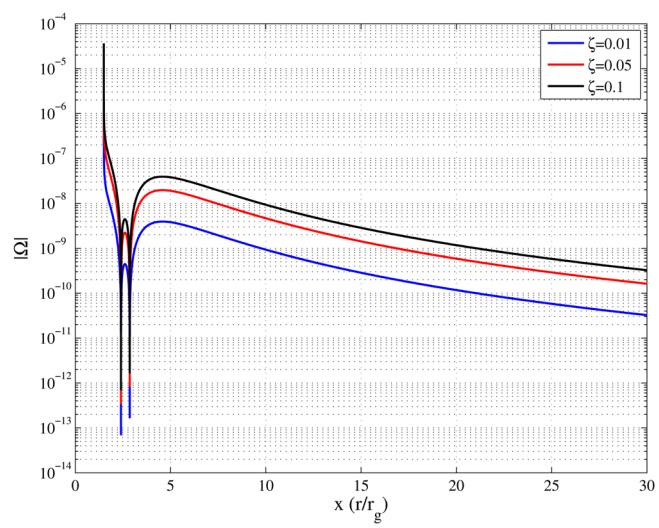

FIG. 4 (color online). Vorticity magnitude (in the units of Gauss) for the Kerr black hole with different ζ values between $1.5r_g$ and $30r_g$ for $M = 14.8M_\odot$ with an accretion rate $\dot{M} = 0.472 \times 10^{19}$ g/s and a = 0.99.

discussion presented in Sec. III, plasma particles in the Schwarzschild accretion disk are described by metric components

$$g_{tt} = -\left(1 - \frac{2r_g}{r} - \frac{R_0}{12}r^2\right) = \alpha^2;$$
$$g_{rr} = \frac{1}{\alpha^2}, \qquad g_{\theta\theta} = r^2; \qquad g_{\phi\phi} = r^2\sin^2\theta, \quad (29)$$

where R_0 is the constant Ricci scalar. First, setting $g_{tt}(r) = 0$, we obtain the condition on the Ricci scalar R_0

$$\mathcal{R}_0 x^3 - 12x + 24 = 0, \quad (30)$$

with $\mathcal{R}_0 = R_0 r_g^2$, $x = r/r_g$, and $\mathrm{a} = a/r_g$. To get a black hole without any naked singularity and with event/cosmological horizons, the solution of Eq. (30) restricts the value for $\mathcal{R}_0$ to be $(-\infty, 4/9)$ ([26]). Further restrictions on $\mathcal{R}_0$ to isolate the geodesics for stable circular orbits can be imposed by demanding $V_{\mathrm{eff}} = 0$, $dV_{\mathrm{eff}}/dr = 0$, and $d^2V_{\mathrm{eff}}/d^2r \geq 0$,

$$\mathcal{R}_0 = \frac{12(6 - x_c)}{(15 - 4x_c)x_c^3}, \quad (31)$$

with x_c being the radius of the stable circular orbit. The above relation also reveals that there exist one innermost and one outermost stable circular orbit, and the upper limit on $\mathcal{R}_0$ reduces to 2.85×10^{-3}. However, the choice of an exact value of $\mathcal{R}_0$ befitting our current analysis depends on the average width, the temperature, and luminosity profiles of black holes. Thus, if the temperature and luminosity profiles prescribed by Page and Thorne [29] are taken into account, it turns out that, for $f(R)$ Schwarzschild black holes, the new range of $\mathcal{R}_0$ further reduces to $(-\infty, 10^{-6}]$. Then the only judicious choice turns out to be $\mathcal{R}_0 = 10^{-6}$, for it satisfies the average radius of the outer edge of a Schwarzschild black hole accretion disk at $r \approx 70r_g$ by setting the innermost and outermost stable circular orbits, according to Eq. (31), at $x_c = 6$ and $x_c = 143.45$ [26].

A similar analysis, carried out for the Kerr metric in modified gravity with the metric elements,

$$g_{tt} = -\alpha^2 = -\frac{(\Delta_r - a^2)}{\Xi^2 r^2}; \qquad g_{rr} = \frac{r^2}{\Delta_r},$$
$$g_{t\phi} = -\frac{2a}{\Xi^2 r^2}(r^2 + a^2 - \Delta_r);$$
$$g_{\phi\phi} = \frac{(r^2 + a^2)^2 - \Delta_r a^2}{\Xi^2 r^2} \quad (32)$$

with

$$\Delta_r = (r^2 + a^2)\left(1 - \frac{R_0}{12}r^2\right) - 2r_g r, \quad (33)$$

$$\Xi = 1 + \frac{R_0}{12}a^2 \quad (34)$$

demands $\mathcal{R}_0$ (upon setting $1/g_{rr} = 0$) to satisfy

$$\left(x^2 + \frac{a^2}{r_g^2}\right)\left(1 - \frac{\mathcal{R}_0 x^2}{12}\right) - 2x = 0. \quad (35)$$

While Eq. (35) yields the range for $\mathcal{R}_0 \in [-0.3, 0.6]$, a new range for $\mathcal{R}_0 \in (0, 0.6]$ emerges if a Kerr black hole with two event horizons and one cosmological horizon is demanded. However, once again, upon demanding $v_{\mathrm{eff}} = 0$, $dV_{\mathrm{eff}}/dr = 0$, and $d^2V_{\mathrm{eff}}/d^2r \geq 0$ along with the appropriate temperature and luminosity profiles mentioned above, we find the stable circular orbits can exist only for $\mathcal{R}_0 \in [-1.2 \times 10^{-3}, 6.67 \times 10^{-4}]$. To maintain the consistency in our numerical plots, we again choose $\mathcal{R}_0 = 10^{-6}$, for it satisfies the average radius of the outer edge of a Kerr black hole accretion disk at $r \approx 16r_g$ by setting the innermost and outermost stable circular orbits at $x_c = 1.4545$ and $x_c = 143.45$, respectively. It should be noted here that temperature profiles used for both classes of accretion disks remain the same as long as we choose $\mathcal{R}_0 \approx 10^{-6}$ [26].

The general expression of vorticity generated in modified gravity is

$$\vec{\Omega}(r) = -(1 + \mathcal{R}_0)\frac{\chi k_b c r \zeta}{q}\frac{1}{\sqrt{g_{rr}g_{\phi\phi}}}\partial_r(\Gamma_m^{-1})(\partial_r T)\Delta t\hat{\theta}, \quad (36)$$

with Γ_m and $\lambda f_m(R) = \mathcal{R}_0$ denoting the modified Lorentz factor and the nonminimal coupling of plasma to $f(R)$ gravity, respectively. Similarly to Eq. (28), we have an analytical expression for modified Schwarzschild space-time,

$$\vec{\Omega}(x) = -(1 + \mathcal{R}_0)\frac{3\zeta k_b \pi \Gamma_m \alpha_m \chi}{q\sqrt{x}r_g}\partial_x T\hat{\theta}, \quad (37)$$

where α_m is associated with modified Schwarzschild metric component g_{tt}.

Figures 5 and 6 show the plot of this generalized vorticity $|\Omega|$ (in the disk) as a function of the distance $x = r/r_g$ in the gravitational field of a black hole of mass $M = 14.8M_\odot$ and $\mathcal{R}_0 = 10^{-6}$. The kinklike behavior of $|\Omega|$ vs $x = r/r_g$, as earlier, originates in the vanishing gradients of temperature and the Lorentz factor. Different values of ζ, used in Figs. 5 and 6, capture the influence of the modified gravity on toroidal temperature fluctuations. Here, it should be emphasized that vorticity magnitude profile in the modified gravity can be drastically different for arbitrary functions of $f(R)$, which signifies how the matter is coupled to its background space-time.

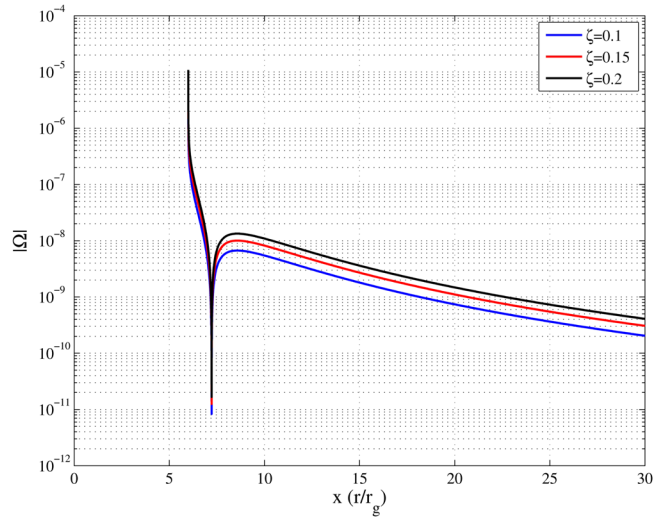

FIG. 5 (color online). Vorticity Ω (in the units of Gauss) for the Schwarzschild black hole with different ζ values in modified gravity within $6.0r_g$ and $30r_g$ for $M = 14.8M_\odot$.

It must be noted that, as maximum temperature obtained in $f(R)$ models turns out to be lower than Cygnus X-1 observation values, the probability of the existence of an accretion disk in the $f(R)$ Schwarzschild black hole becomes very slim [32]. Still we present the result here for $f(R)$ Schwarzschild black hole as an analytical example.

E. Relative strength of relativistic and baroclinic drive

The generalized magnetofluid dynamics, derived for a barotropic equation of state, will have only the relativistic vorticity drives. We would now like to compare the relative magnitudes of the relativistic, and possibly baroclinic, vorticity sources. At first glance, it is evident (from the metric) that the relativistic source will dominate the baroclinic source as we approach the event horizon. But to make a comparison between the relativistic and baroclinic drives, let us construct a simple baroclinic drive of the form $\nabla T \times \nabla \sigma \approx (\epsilon/r) g_{\phi\phi}^{-1/2} \partial_\phi (k_b T)$, where ϵ is a measure of the departure from strict barotropic behavior. The preceding approximation introduces a smaller toroidal temperature variation that quantifies the nonbarotropic component.

In Figs. 7 and 8, we compare the relative strength of the relativistic and baroclinic drive for black hole accretion disks in Schwarzschild and Kerr geometries. We plot the relative magnitude as a function of the radial distance, $x = r/r_g$; both plots start from their respective isco. In both cases, the relativistic drive becomes dominant as we approach the innermost stable orbit. For smaller values of ϵ, we see the magnitude of the relativistic drive keeps increasing as the departure from barotropic fluid is minimal. Also, the dashed line shows the ratio to be unity, and from both figures we see that the relativistic drive remains dominant, for smaller values of ϵ; the dominance continues to longer distances from the innermost stable circular orbit. In both cases, the Lorentz factor plays an important role in determining their relative strength. Thus, the sudden dip in the relative strength profile in Kerr metric can be attributed to the vanishing gradient of the corresponding Lorentz factor inherent in the relativistic drive. Moreover, the relative magnitude in the Kerr black hole is less than that in Schwarzschild black hole because of the significant energy loss of plasmas in Kerr space-time due to gravitational radiation reaction as it approaches the nonstable

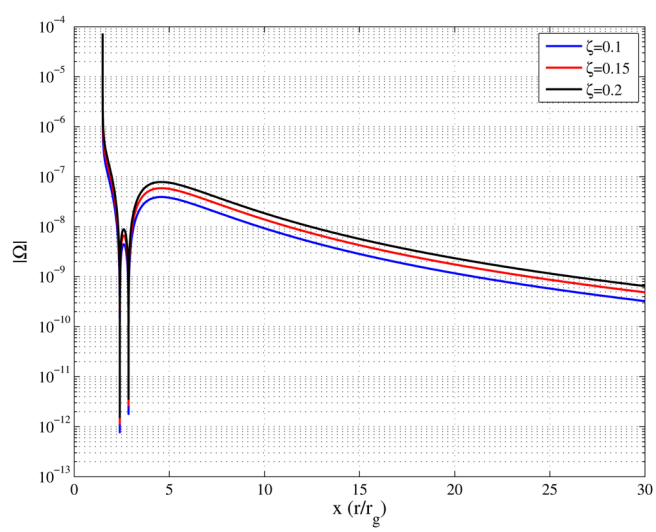

FIG. 6 (color online). Vorticity Ω (in the units of Gauss) for the Kerr black hole with different ζ values in modified gravity within $1.5r_g$ and $30r_g$ for $M = 14.8M_\odot$ with an accretion rate $\dot{M} = 0.472 \times 10^{19}$ g/s and a = 0.99.

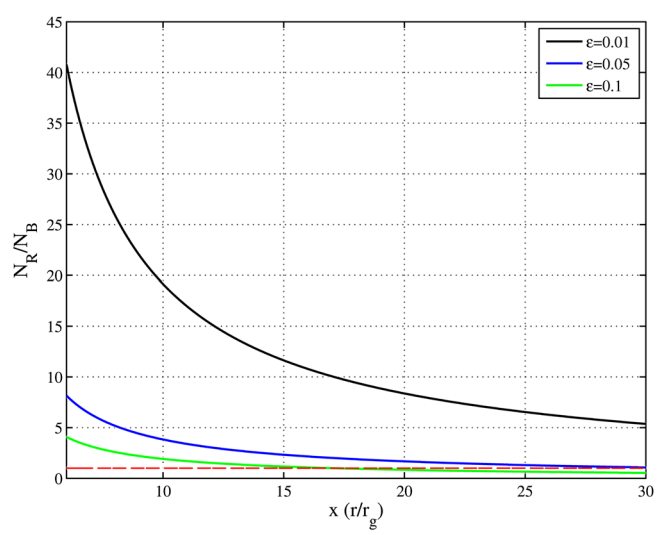

FIG. 7 (color online). Ratio between relativistic and baroclinic drive in Schwarzschild black hole with $\epsilon = 0.01$ (black), 0.05 (green), and 0.1 (blue). The red line represents the ratio of unity.

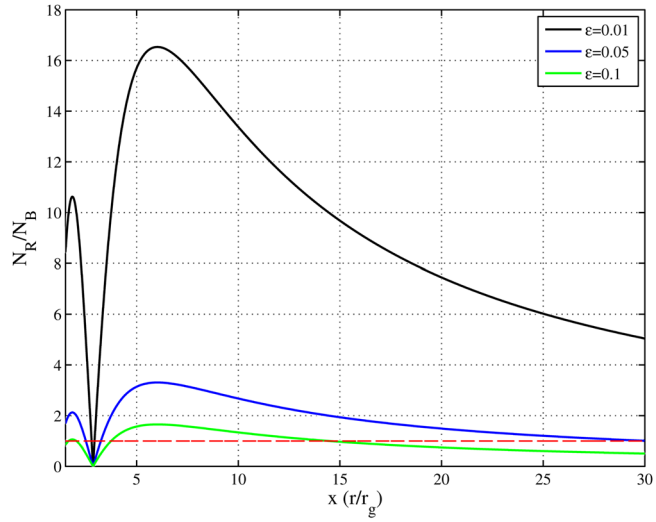

FIG. 8 (color online). Ratio between the relativistic and baroclinic drive in the Kerr black hole with $\epsilon = 0.01$ (black), 0.05 (green), and 0.1 (blue). The red line represents the ratio of unity.

orbits. The jump in relative intensity from $\epsilon = 0.01$ to $\epsilon = 0.05$ remains significant in both geometries.

IV. CONCLUSION

We have explored in this paper the possibility of generating what may be called "generalized vorticity" in accretion disks surrounding compact gravitating objects, in particular, the Kerr and Schwarzschild black holes. The accretion disc plasma is coupled nonminimally [via $f(R)$ gravity] to the surrounding specified space-time. Although vorticity can be generated by the well-known baroclinic mechanism (nonzero $\nabla T \times \nabla \sigma$), we have concentrated, in this paper, on exploring what are classed as relativistic drives stemming from space-time distortions caused by special as well as general relativistic effects. We find that the Kerr geometry, due to the intrinsic rotation, is a more efficient vorticity generator as compared to the Schwarzschild counterpart. We also observe a slight increase in vorticity generation even if an extremely weak $f(R)$ (nonminimal) coupling, $f(R) = R_0 =$ constant, is turned on, which implies that a noticeable change in vorticity generation will be observed in strong $f(R)$ coupling. Physically, the increase in efficiency is directly related to the amount of deviation from the circular orbits (of the plasma particles) caused by the distorted geometry.

We also compared the efficiency of the relativistic drive with a model baroclinic drive. The strength of the baroclinic drive is given in terms of a parameter ϵ, that measures the departure from strict barotropy. For most accretion disk plasmas in quasiequilibrium, ϵ is expected to be small. We find that, for reasonable values of ϵ, the relativistic drive is dominant for the disk regions nearer to the compact object; as the distance increases, and for relatively larger ϵ, the barcolinic term becomes comparable to the relativistic drive. This vorticity growth occurs in the orbital time scale, similar to MRI instability, which later can amplify through several dynamo mechanisms [33–35].

Unlike GR-Magnetohydrodynamics, our formalism can be extended to multifluid species with each species obeying its own vortical dynamics [36,37]. In addition, the induction equation in this formalism has source terms for vorticity generation; these sources can catapult the accretion disk to a state of finite vorticity from one with no vorticity (electromagnetic and hydrodynamic). This formalism can also be studied in the context of vortex generation in the protoplanetary disks near a supermassive star where gravity plays a dominant role. Hyrdodynamic simulations indicate these protoplanetary disks to be inherently baroclinic due to a negative radial entropy gradient [7,13,35]. The turbulence caused by the baroclinic instabilities is found to be suitable for angular momentum transport and vortex formation in the disk which are suggested to lead to planet formation. Our model, if applied to the evolution of the protoplanetary disk, will provide additional sources for angular momentum transport and vortex formation even in a barotropic disk.

Regardless of the details, the curvature drive (in minimal as well as in nonminimal gravity) will always generate "generalized" vorticity which, either by itself or after amplification through a generalized dynamo mechanism, can provide a mechanism for angular momentum transport. These amplified vortical fields can also collimate the jets emanating from the disk where field lines corotate with the disk, by the flux freezing theorem. The plasma leaving the disk can drag the field lines due to its large conduction coefficient which wraps the field lines around the rotation axis. The field lines then exert a radial force which can compress the jet of plasma leading to jet collimation [2].

ACKNOWLEDGMENTS

Authors thank David J. Stark and Manasvi Lingam for helpful discussions. C. B. and S. M. M.'s research was supported by the US DOE Grant No. DE-FG02-04ER-54742.

APPENDIX: 3 + 1 DYNAMICS OF GRAVITOMAGNETOFLUID

The approach chosen for the $3+1$ splitting selects a family of foliated fiducial three-dimensional hypersurfaces (slices of simultaneity) Σ_t labelled by a parameter $t =$ constant in terms of a time function on the manifold. Furthermore, we let t^μ be a timeline vector of which the integral curves intersect each leaf Σ_t of the foliation precisely once and which is normalized such that $t^\mu \nabla_\mu t = 1$. This t^μ is the "evolution vector field" along the orbits of which different points on all $\Sigma_t \equiv \Sigma$ can be identified. This allows us to write all space-time fields in

terms of t-dependent components defined on the spatial manifold Σ_t. Lie derivatives of space-time field along t^μ are identified with "time derivatives" of the spatial fields since Lie derivatives reduce to a partial time derivative for an adapted coordinate system $t^\mu = (1, 0, 0, 0)$.

Moreover, since we are using the Lorentzian signature, the vector field t^μ is required to be future directed. Let us decompose t^μ into normal and tangential parts with respect to Σ_t by defining the lapse function α and the shift vector β^μ as $t^\mu = \alpha n^\mu + \beta^\mu$ with $\beta^\mu n_\mu = 0$, where n^μ is the future directed unit normal vector field to the hypersurfaces Σ_t. More precisely, the natural timelike covector $n_\mu = (-\alpha, 0, 0, 0) = -\alpha \nabla_\mu t$ is defined to obtain $n^\mu = (1/\alpha, -\beta^\mu/\alpha)$ which satisfies the normalization condition $n^\mu n_\mu = -1$. Then, the space-time metric $g_{\mu\nu}$ induces a spatial metric $\gamma_{\mu\nu}$ by the formula $\gamma_{\mu\nu} = g_{\mu\nu} + n_\mu n_\nu$. Finally, the $3+1$ decomposition is usually carried out with the projection operator $\gamma^\mu{}_\nu = \delta^\mu{}_\nu + n^\mu n_\nu$, which satisfies the condition $n^\mu \gamma_{\mu\nu} = 0$. Also, the acceleration is defined as $a_\mu = n^\nu \nabla_\nu n_\mu$.

Now, with the above foliation of space-time, the space-time metric takes the canonical form [20]

$$ds^2 = -\alpha^2 dt^2 + \gamma_{ij}(dx^i + \beta^i dt)(dx^j + \beta^j dt), \tag{A1}$$

and it immediately follows that, with respect to an Eulerian observer, the Lorentz factor turns out to be

$$\Gamma = [\alpha^2 - \gamma_{ij}(\beta^i \beta^j + 2\beta^i v^j + v^i v^j)]^{-1/2}, \tag{A2}$$

satisfying $d\tau = dt/\Gamma$, where v^i is the ith component of fluid velocity $\vec{v} = d\vec{x}/dt$. Then the decomposition for the 4-velocity is [14]

$$U^\mu = \alpha \Gamma n^\mu + \Gamma \gamma^\mu{}_\nu v^\nu, \tag{A3}$$

with $n_\mu U^\mu = -\alpha\Gamma$.

Now, since our unified antisymmetric field tensor $\mathcal{M}^{\mu\nu}$ is constructed from the antisymmetric tensors $F^{\mu\nu}$ and $D^{\mu\nu}$, we apply the ADM formalism of electrodynamics presented in Refs. [20–23] to define the generalized electric and magnetic fields, respectively, as

$$\xi^\mu = n_\nu \mathcal{M}^{\mu\nu}; \qquad X^\mu = \frac{1}{2} n_\rho \epsilon^{\rho\mu\sigma\tau} \mathcal{M}_{\sigma\tau}, \tag{A4}$$

and thus express the unified field tensor

$$\mathcal{M}^{\mu\nu} = n^\mu \xi^\nu - n^\nu \xi^\mu - \epsilon^{\mu\nu\rho\sigma} X_\rho n_\sigma. \tag{A5}$$

We remind the reader that the generalized magnetic field and the generalized vorticity are essentially synonymous. Using the definition of the unified field tensor $\mathcal{M}^{\mu\nu}$, the expressions of 3D generalized electric and magnetic fields turn out to be

$$\begin{aligned}\vec{\xi} = \vec{E} &- \frac{m}{q}(1 + \lambda f_m(R) - \lambda R F_m(R))\vec{\nabla}(\alpha \mathcal{G}\Gamma) \\ &- \frac{m}{q}\lambda F_m(R)\vec{\nabla}(\alpha \mathcal{G} R \Gamma) \\ &- \frac{m}{q}(1 + \lambda f_m(R))\left[2\underline{\underline{\sigma}} \cdot (\mathcal{G}\Gamma\vec{v}) + \frac{2}{3}\Theta \mathcal{G}\Gamma\vec{v}\right] \\ &- \frac{m}{q\alpha}(1 + \lambda f_m(R) - \lambda R F_m(R))(\mathcal{L}_t(\mathcal{G}\Gamma\vec{v}) - \mathcal{L}_{\vec{\beta}}(\mathcal{G}\Gamma\vec{v})) \\ &- \frac{m}{q\alpha}\lambda F_m(R)(\mathcal{L}_t(\mathcal{G}R\Gamma\vec{v}) - \mathcal{L}_{\vec{\beta}}(\mathcal{G}R\Gamma\vec{v}));\end{aligned} \tag{A6}$$

$$\begin{aligned}\vec{X} = \vec{B} &+ \frac{m}{q}(1 + \lambda f_m(R) - \lambda R F_m(R))\vec{\nabla} \times (\mathcal{G}\Gamma\vec{v}) \\ &+ \lambda F_m(R)\frac{m}{q}\vec{\nabla} \times (R\mathcal{G}\Gamma\vec{v}),\end{aligned} \tag{A7}$$

where $\underline{\underline{\sigma}} = \sigma^\nu_\mu$ and Θ are, respectively, the shear and expansion of the congruence, defined as $\sigma_{\alpha\beta} = \gamma^\mu_\alpha \gamma^\nu_\beta \nabla_{(\mu} n_{\nu)} - \frac{1}{3}\theta\gamma_{\mu\nu}$ and $\Theta = \nabla_\mu n^\mu$. We have also used the relation $\nabla_\mu n_\nu = -a_\nu n_\mu + \sigma_{\alpha\beta} + \frac{1}{3}\theta\gamma_{\mu\nu}$ to derive (A6).

[1] S. L. Shapiro and S. A. Teukolsky, *Blackholes, White Dwarfs and Neutron Stars* (University of Chicago, Chicago, 1984).

[2] M. Vietri, *Foundations of High Energy Astrophysics* (University of Chicago, Chicago, 2008).

[3] X. Cao and H. C. Spruit, The large-scale magnetic fields of thin accretion disks, Astrophys. J. **765**, 149 (2013).

[4] M. A. Abramowicz and P. C. Fragile, Foundations of black hole accretion disk theory, Living Rev. Relativiy **16**, 1 (2013).

[5] M. C. Begelman, R. D. Blandford, and M. J. Rees, Theory of extragalactic radio sources, Rev. Mod. Phys. **56**, 255 (1984).

[6] J. H. Krolik, *Active Galactic Nuclei: From the Central Black Hole to the Galactic Environment* (Princeton University, Princeton, NJ, 1999).

[7] H. H. Klahr and P. Bodenheimer, Turbulence in accretion disks. Vorticity generation and angular momentum transport via the global baroclinic instability, Astrophys. J. **582**, 869 (2003).

[8] M. R. Petersen, K. Julien, and G. R. Stewart, Baroclinic vorticity production in protoplanetary disks. I. Vortex formation, Astrophys. J. **658**, 1236 (2007).

[9] M. R. Petersen, G. R. Stewart, and K. Julien, Baroclinic vorticity production in protoplanetary disks. II: Vortex growth and longevity, Astrophys. J., **658**, 1252 (2007).

[10] R. M. Kulsrud, R. Cen, J. P. Ostriker, and D. Ryu, The protogalactic origin for cosmic magnetic fields, Astrophys. J. **480**, 481 (1997).

[11] J. F. Hawley and S. A. Balbus, The dynamical structure of nonradiative black hole accretion flows, Astrophys. J. **573**, 738 (2002).

[12] S. A. Balbus and J. F. Hawley, Instability, turbulence, and enhanced transport in accretion disks, Rev. Mod. Phys. **70**, 1 (1998).

[13] N. Raettig, W. Lyra, and H. Klahr, A parameter study for baroclinic vortex amplification, Astrophys. J. **765**, 115 (2013).

[14] F. A. Asenjo, S. M. Mahajan, and A. Qadir, Generating vorticity and magnetic fields in plasmas in general relativity: Spacetime curvature drive, Phys. Plasmas **20**, 022901 (2013).

[15] S. M. Mahajan, Temperature-Transformed 'Minimal Coupling': Magnetofluid Unification, Phys. Rev. Lett. **90**, 035001 (2003).

[16] J. D. Bekenstein, Helicity conservation laws for fluids and plasmas, Astrophys. J. **319**, 207 (1987).

[17] S. M. Mahajan and Z. Yoshida, Twisting Space-Time: Relativistic Origin of Seed Magnetic Field and Vorticity, Phys. Rev. Lett. **105**, 095005 (2010).

[18] S. M. Mahajan and Z. Yoshida, Relativistic generation of vortex and magnetic field a), Phys. Plasmas **18**, 055701 (2011).

[19] C. Bhattacharjee, R. Das, and S. M. Mahajan, Magnetofluid dynamics in curved spacetime, Phys. Rev. D **91**, 064055 (2015).

[20] A. J. Wheeler, C. W. Misner, and K. S. Thorne, *Gravitation* (Freeman, San Francisco, 1973).

[21] K. S. Thorne and D. MacDonald, Electrodynamics in curved spacetime: $3+1$ formulation, Mon. Not. R. Astron. Soc. **198**, 339 (1982).

[22] R. M. Wald, *General Relativity* (University of Chicago, Chicago, 1984).

[23] K. S. Thorne, R. H. Price, and D. A. MacDonald, *Black Holes: The Membrane Paradigm* (Yale University, New Haven, CT, 1986).

[24] P. Chang and L. Hui, Stellar structure and tests of modified gravity, Astrophys. J. **732**, 25 (2011).

[25] A.-C. Davis, E. A. Lim, J. Sakstein, and D. J. Shaw, Modified gravity makes galaxies brighter, Phys Rev. D **85**, 123006 (2012).

[26] D. Pérez, G. E. Romero, and S. E. Perez Bergliaffa, Accretion disks around black holes in modified strong gravity, Astron. Astrophys., **551**, A4 (2013).

[27] T. Harko, Z. Kovács, and F. S. N. Lobo, Thin accretion disks in stationary axisymmetric wormhole spacetimes, Phys. Rev. D **79**, 064001 (2009).

[28] I. D. Novikov and K. S. Thorne, in *Astrophysics of black holes*, edited by C. Dewitt, B. S. Dewitt, Black Holes (Les Astres Occlus, 1973), pp. 343–450.

[29] D. N. Page and K. S. Thorne, Disk-accretion onto a black hole. time-averaged structure of accretion disk, Astrophys. J. **191**, 499 (1974).

[30] A. Skadowski, M. Abramowicz, M. Bursa, W. Kluźniak, J.-P. Lasota, and A. Różańska, Relativistic slim disks with vertical structure, Astron. Astrophys. **527**, A17 (2011).

[31] J. A. Orosz, J. E. McClintock, J. P. Aufdenberg, R. A. Remillard, M. J. Reid, R. Narayan, and L. Gou, The mass of the black hole in cygnus x-1, Astrophys. J. **742**, 84 (2011).

[32] L. Gou, J. E. McClintock, M. J. Reid, J. A. Orosz, J. F. Steiner, R. Narayan, J. Xiang, R. A. Remillard, K. A. Arnaud, and S. W. Davis, The extreme spin of the black hole in cygnus x-1, Astrophys. J. **742**, 85 (2011).

[33] M. Marklund and C. A. Clarkson, The general relativistic magnetohydrodynamic dynamo equation, Mon. Not. R. Astron. Soc. **358**, 892 (2005).

[34] M. Reinhardt and A. Rosenblum, A note on general relativistic dynamo mechanisms, Phys. Lett. A **53**, 269 (1975).

[35] H. Klahr, The global baroclinic instability in accretion disks. 2: Local linear analysis, Astrophys. J. **606**, 1070 (2004).

[36] J. C. McKinney, A. Tchekhovskoy, and R. D. Blandford, General relativistic magnetohydrodynamic simulations of magnetically choked accretion flows around black holes, Mon. Not. R. Astron. Soc. **423**, 3083 (2012).

[37] R. F. Penna, J. C. McKinney, R. Narayan, A. Tchekhovskoy, R. Shafee, and J. E. McClintock, Simulations of magnetized discs around black holes: Effects of black hole spin, disc thickness and magnetic field geometry, Mon. Not. R. Astron. Soc. **408**, 752 (2010).